Scientific Research and Essays Vol. 6(28), pp. 5883-5894, 23 November, 2011
Available online at http://www.academicjournals.org/SRE
DOI: 10.5897/SRE11.904
ISSN 1992-2248 © 2011 Academic Journals

Full Length Research Paper

InP-based multi-quantum-well mole fraction variation effects on a double wafer-fused GaAs/InP LW-VCSEL

P Susthitha Menon* and Sahbudin Shaari

Institute of Microengineering and Nanoelectronics (IMEN),University Kebangsaan Malaysia (UKM), 43600 UKM Bangi, Selangor, Malaysia.

Accepted 27 July, 2011

We analyze the effects of the mole fraction variation of III-V heterostructures employed as the active region in an InP-based multi-quantum-well (MQW), long-wavelength vertical-cavity surface-emitting laser (LW-VCSEL). The VCSEL model which utilizes an air-post design for electrical current confinement is equipped with GaAs/AlGaAs and GaAs/AlAs top and bottom distributed Bragg reflectors(DBR) mirrors respectively. The changes in the quantum well band-gap energy is evaluated against the laser performance in terms of its threshold current, gain, lasing wavelength and emission power by means of an industrial-based numerical simulator. The simulated device achieved lasing powers up to 4.9 mW with modal gain of 25 cm^{-1}, lasing wavelength of 1.56 µm and threshold current <0.8 mA for $In_{1-x}Ga_xAs_yP_{1-y}$ quantum well (QW) and quantum well barrier (QWB) mole fraction of x_{QW} = 0.24, y_{QW} = 0.82, x_{QWB} = 0.52 and y_{QWB} = 0.82. Results from this work is beneficial for optical design engineers to determine the appropriate material to be used in the active region of a LW-VCSEL.

Key words: LW-VCSEL, mole fraction, wafer-fused, multi-quantum-well, InGaAsP.

INTRODUCTION

Long-wavelength vertical-cavity surface-emitting lasers (LW-VCSELs) operating at 1.3 and 1.55 µm have been extensively studied during the last decade. Their circular and spatial single-mode beam provides very efficient fiber coupling and makes them very attractive light sources for telecommunication especially for coarse wavelength division multiplexing (CWDM) applications in metro and local access networks such as fiber-to-the home (FTTH) (Karim et al., 2001). The optical line terminal (OLT) and optical network unit (ONU) transceiver modules in FTTH networks would benefit much in having small form factors with limited power budgets but with energy-efficient LW-VCSELs (Hofmann, 2011).

VCSELs comprise of an active region sandwiched between top and bottom distributed Bragg reflectors (DBRs). The active region comprises of multi quantum wells formed by alternately stacking thin layers of wider and narrower band-gaps thereby creating a series of potential wells. As the dimensions of the potential wells are reduced to the order of 10 nm, the movement of electrons is restricted inside the potential well and quantum effects become prominent. The quantum well effect makes it possible to tailor the shapes of the gain function of a VCSEL so that it is peaked at a specified frequency. A semiconductor laser using the quantum well effect has advantageous features such as narrow frequency band gain curve, lower threshold current, less temperature dependence and frequency of emission that can be designed by the dimension of the wells (Iizuka 2002; Qi et al., 2010).

Currently, there are three main approaches being used in LW-VCSEL design. The first approach is an all-epitaxial wafer comprising of quarter-wavelength layers of InAlGaAs/InAlAs (InP) top and bottom distributed Bragg reflectors (DBRs) and active cavity region. In the second approach an InAlGaAs/InAlAs(InP) DBR is combined with a dielectric DBR. And finally, in the third approach, the

*Corresponding author. E-mail: susi@eng.ukm.my. Tel: +6-03-89217151. Fax: +6-03-89259080.

InAlGaAs/InP active cavity is combined with wafer-fused AlGaAs/GaAs DBRs. For each one of these approaches, the maximum single-mode output power was 0.5 mW (70°C), 1.4 mW (80°C) and 2.5 mW respectively(80°C) (Kapon and Sirbu, 2009). Fabrication of LW-VCSEL using the wafer fusion method can be achieved using either InGaAsP, InGaAlAs or AlInGaAs as the active region in the multi quantum well (MQW) layer (Karim et al., 2001; Mehta et al. 2006; Hofmann and Amann 2008; Mereuta et al., 2009). The highest output power obtained for these devices was 0.65 mW (20°C), power density of 130 W/cm^2 (70°C) and 2.5 mW respectively.

In this paper, we explore the effects of the multi quantum well mole fraction towards the characteristics of a wafer-bonded InP-based LW-VCSEL by means of an industrial-based simulator. Details of other characterization results can be obtained from our past work (Menon et al., 2011; Menon et al., 2010a, b, c; Kumarajah et al., 2009a, b).

MATERIALS AND METHODS

Theoretical analysis

The numerical analysis tool uses a comprehensive set of equations to derive the electrical, optical and thermal phenomenon that takes place within the device. These include the Poisson's equation, carrier continuity equations, Helmholtz equation, the photon-rate equation and the heat flow equation (Menon et al., 2010a)

In this paper, in addition to the equations stipulated earlier, two main equations that will be used are the Schrodinger's equation and the default energy band-gap equation for InP-based material. The energy levels E_q of a particle of mass m confined to a one-dimensional infinite rectangular well of full width d are determined by solving the time-independent Schrodinger equation (Li and Iga 2002).

$$E_q = \frac{\hbar (q\pi / d)^2}{2m} \quad (1)$$

where q=1,2,……. This means the smaller the width of the quantum well, the larger the separation between adjacent energy levels.
The default energy band-gap for the InP lattice matched $In_{1-x}Ga_xAs_yP_{1-y}$ system used in this modeling is given by (Silvaco, 2010):

$$E_g = 1.35 + (0.642 + 0.758x)x + (0.101y - 1.101)y - (0.28x - 0.109y + 0.159)xy \quad (2)$$

where x and y are the respective mole fraction for the III-V material.

Device design

Figure 1 shows the simulated design of the air-post wafer-bonded GaAs-based 1.5 µm VCSEL device. In this structure, the multi-quantum well (MQW) active region consists of six 5.5 nm thick $In_{0.76}Ga_{0.24}As_{0.82}P_{0.18}$ quantum wells and 8 nm thick $In_{0.48}Ga_{0.52}As_{0.82}P_{0.18}$ barriers. The MQWs are embedded in InP spacer layers that have been extended by thin GaAs layers on top of each fused mirror to increase emission wavelength. Alternating high- and low-refractive index layers of GaAs/$Al_{0.33}Ga_{0.67}As$ form the top 30-period p-type DBR whereas the bottom n-type DBR mirror is formed with 28-periods of GaAs/AlAs layers.

RESULTS

The $In_{1-x}Ga_xAs_yP_{1-y}$ mole fraction was varied from 0.14 to 0.94 for the quantum well material's x component (x_{QW}) whereas variation was made from 0.12 till 0.92 for the x and y components (y_{QW}, x_{QWB}, y_{QWB}) of the quantum well barrier material while keeping the other mole fraction components constant at their default values. The effects of these variation on the LW-VCSEL's characteristics such as the power-current (L-I), gain-current, wavelength-current (λ-I) and the threshold current (I_{th}) was analyzed and is explained henceforth.

Figures 2 to 5 displays the effects of variation in the x component of the mole fraction of the quantum well material. Between a range of x_{QW} = 0.14 till x_{QW} = 0.94, lasing only occurs for x_{QW}=0.14, 0.24 and 0.34 where at the maximum voltage of 3 V, the equivalent lasing power (current) is 0.02 mW (17.1 mA), 4.8 mW (14.7 mA) and 4.7 mW (13.3 mA) respectively. The differential series resistance and conversion efficiency is at 174 Ω (0.04%), 203 Ω (10.9%) and 225 Ω (11.8%). The modal gain and lasing wavelength is maintained constant at 25 cm^{-1} and 1.56 µm respectively. It is a well known fact that multi quantum wells are formed by alternately stacking thin layers of wider and narrower band-gaps thereby creating a series of potential wells. Therefore, Figure 5 explains the reason for the non-lasing behavior of the other x component mole fraction values of the quantum well material. For x_{QW}<0.44, the quantum well band gap energy (hyphenated line, right y-axis values) is significantly narrower (19 to 36% lower) than the barrier band-gap energy (dotted line, right y-axis) allowing for stimulated recombination and lasing to occur. The threshold current (diamond-bulleted line, left y-axis) is <0.8 mA.

Similarly, Figures 6 to 9 displays the effect of variation in the y component of the mole fraction of the quantum well material. Lasing only occurs for y_{QW} = 0.82 and 0.92 where at the maximum voltage of 3 V, the equivalent lasing power (current) is 4.7 mW (13.3 mA) and 4.8 mW (14.7 mA). The differential series resistance and conversion efficiency is at 225 Ω (11.8%) and 199 Ω (11.1%). The modal gain and lasing wavelength is maintained constant at 25 cm^{-1} and 1.56 µm respectively. Likewise Figures 5 and 9 portrays the threshold current (left y-axis) for different values of the mole fraction where lasing only occurs for quantum well band-gap energies (right y-axis) which are much narrower than the quantum well barrier band-gap energy (28 to 38% lower). The achieved threshold current is 0.19 mA (y_{QW} = 0.82) and 0.7 mA (y_{QW} = 0.92) respectively.

The quantum well barrier material mole fraction

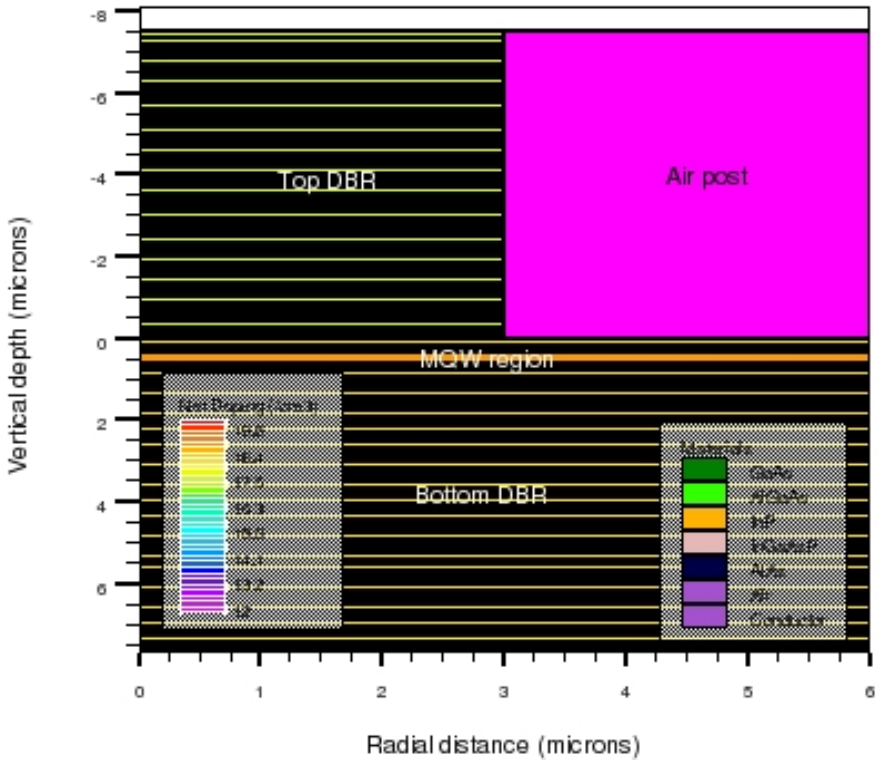

Figure 1. Simulated two dimensional cross-section view of the double wafer-fused GaAs/InP-based LW-VCSEL.

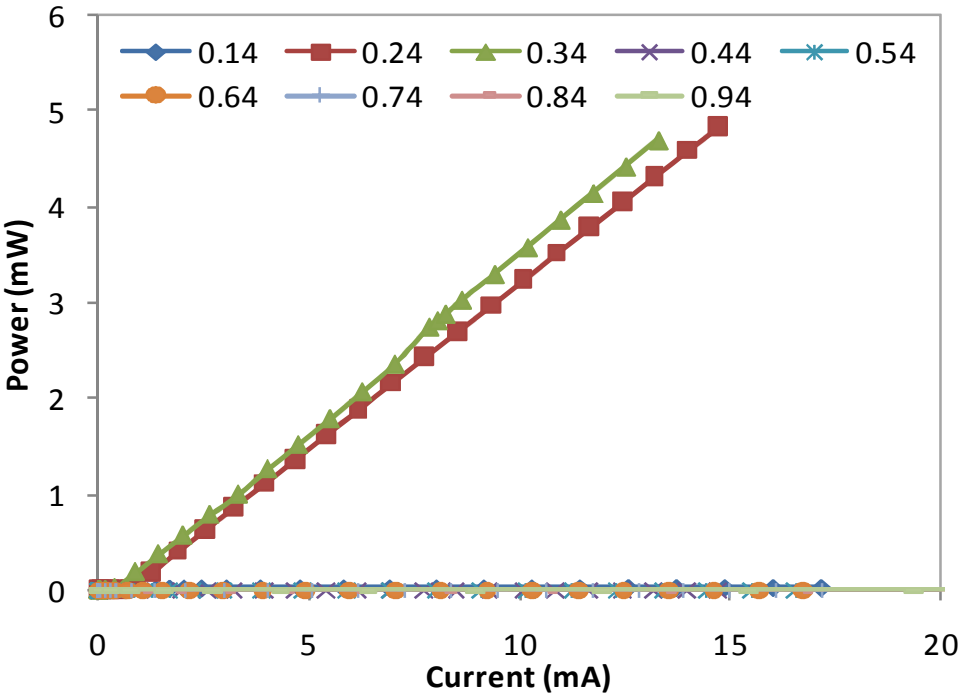

Figure 2. L-I curve for QW x component variation.

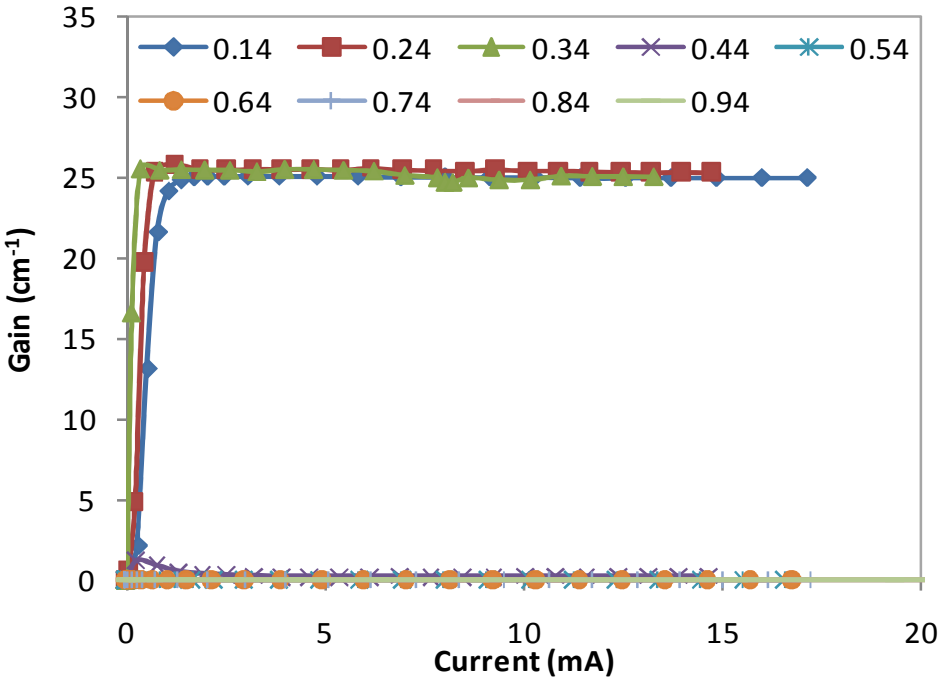

Figure 3. Gain-I curve for QW x component variation.

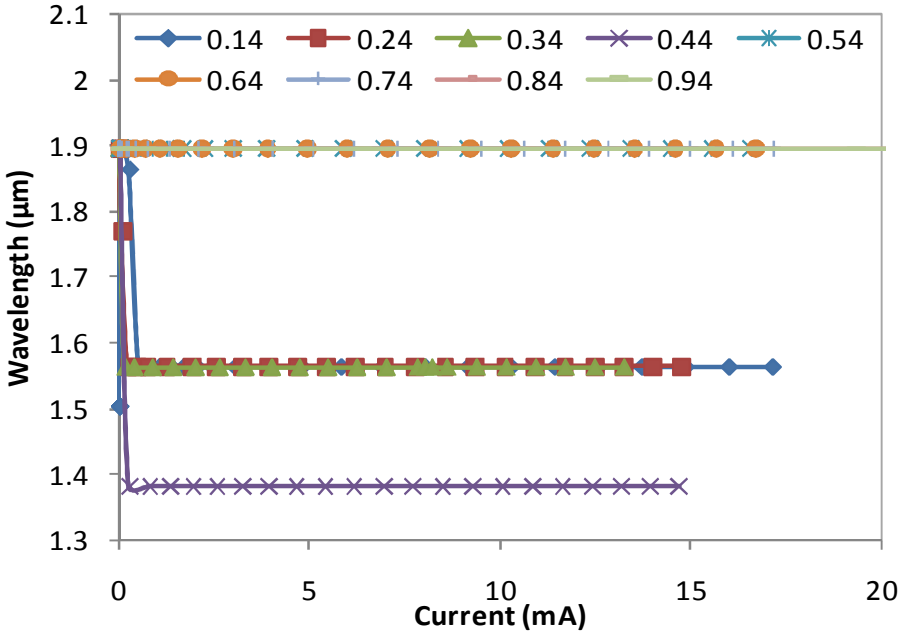

Figure 4. λ-I curve for QW x component variation.

variation effects is analyzed in Figures 10 to 17. Lasing only occurs when x_{QWB} = 0.42, 0.52 and 0.62 as well as when y_{QWB} = 0.72, 0.82 and 0.92. The lasing power decreases from 4.9 mW to 3.78 mW for x_{QWB} = 0.42 till x_{QWB} = 0.62 whereas increment in lasing power from 3.8 mW to 4.9 mW is observed for y_{QWB}=0.72 till y_{QWB} = 0.92.

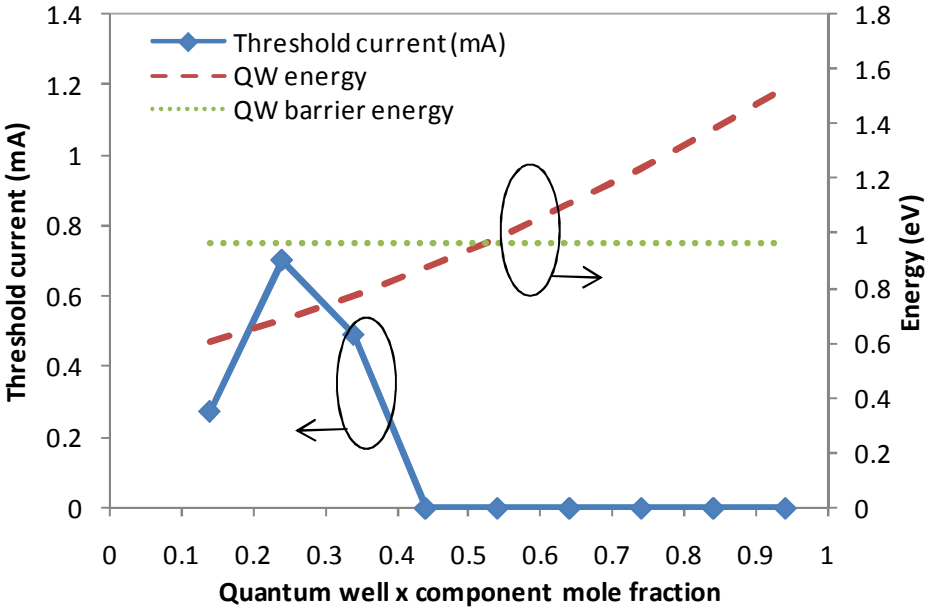

Figure 5. I_{th} (diamond bulleted line, left y-axis) and band gap energy (dotted and hyphenated lines, right y-axis) variation for different QW x component mole fraction variation.

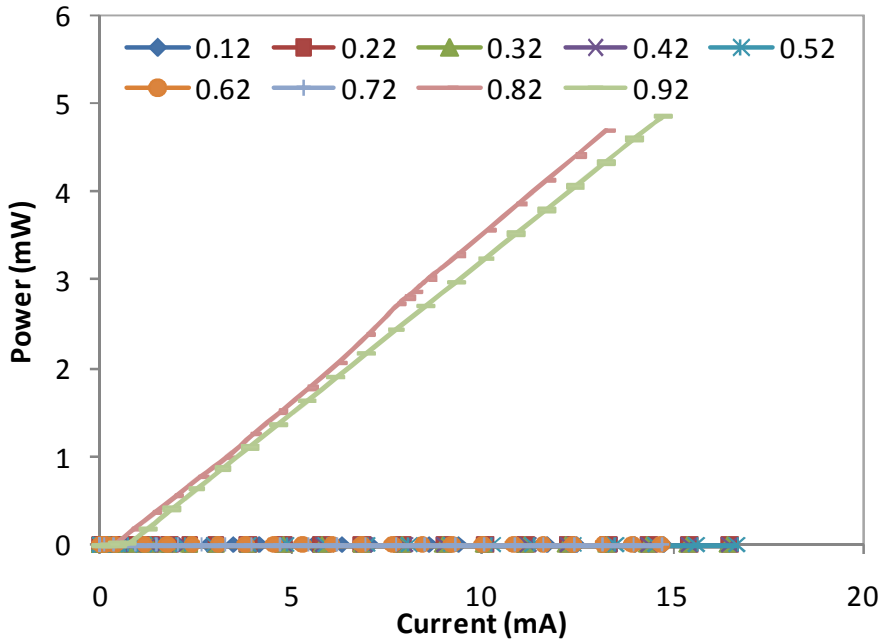

Figure 6. L-I curve for QW y component variation.

Lower quantum well barrier band-gap energies produce higher lasing power as it allows electron tunneling to take place between adjacent quantum wells. The modal gain and lasing wavelength is maintained at 25 cm^{-1} and 1.56 μm respectively. Figures 13 and 17 also show that threshold current of <0.8 mA is achieved for quantum well barrier material with band-gap energies (right y-axis) that are 19 to 36% higher than the quantum well band-gap

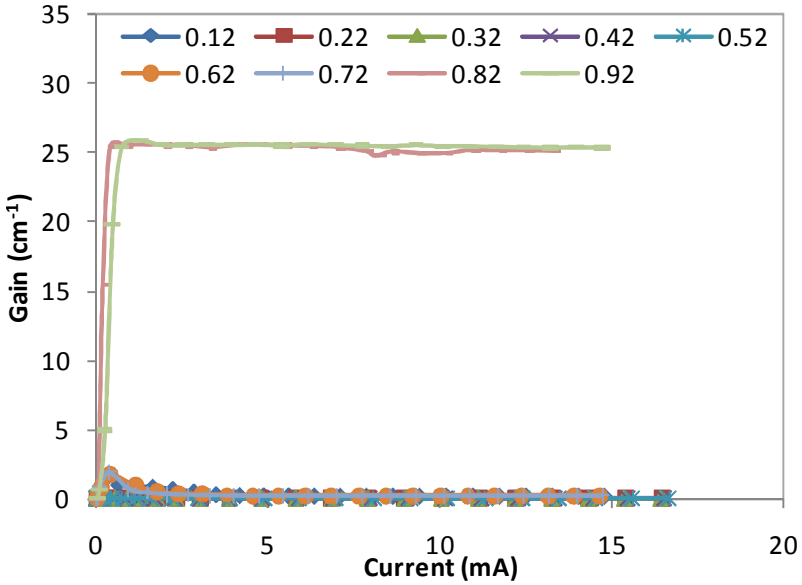

Figure 7. Gain-I curve for QW y component variation.

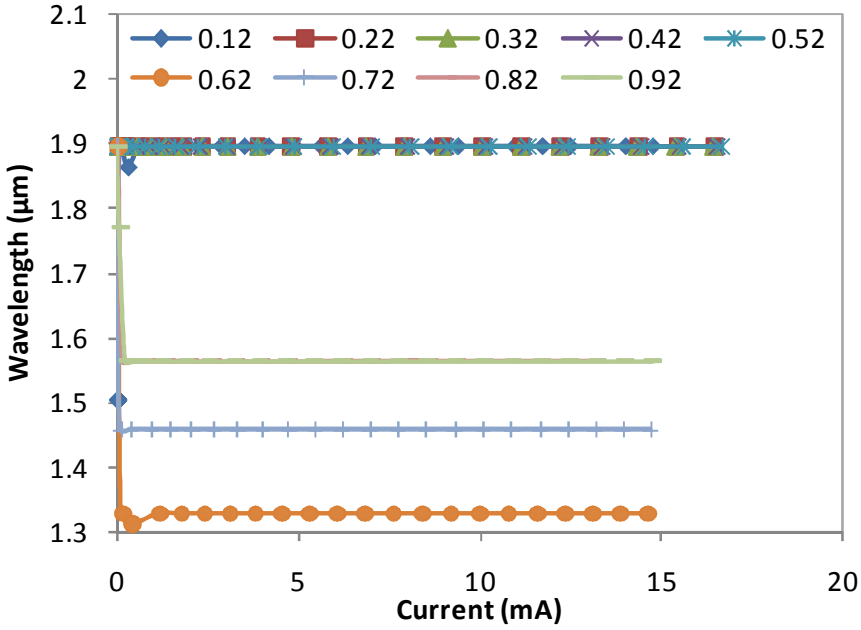

Figure 8. λ-I curve for QW y component variation.

energy. The threshold current (left y-axis) is again <0.8 mA.

DISCUSSION

From the results, it has been shown that lasing in a LW-VCSEL only occurs for certain combinations of x and y mole fractions for both the quantum well and quantum well barrier. The main criteria is for the quantum well barrier band-gap energy to be higher than the quantum well band-gap energy since a lower quantum well band-gap energy enables optical recombination to take place in the quantum well region to produce the stimulated

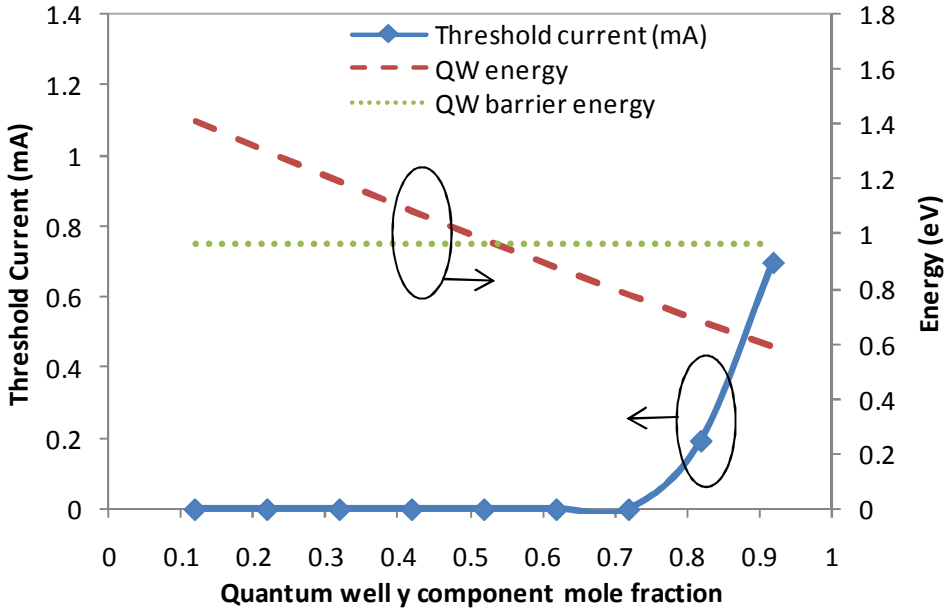

Figure 9. I_{th} (diamond bulleted line, left y-axis) and band gap energy (dotted and hyphenated lines, right y-axis) variation for different QW y component mole fraction variation.

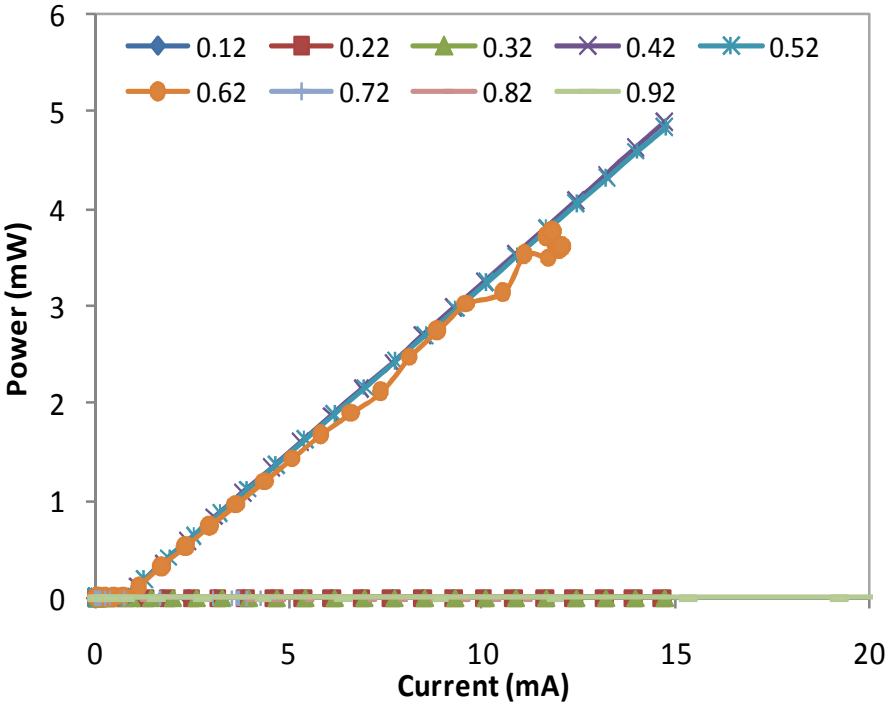

Figure 10. L-I curve for QW barrier x-comp variation.

emission process. A higher quantum well barrier band-gap energy ensures that no carrier tunneling occurs between quantum wells and repeatable optical recombination occurs from the carriers that arrive at the

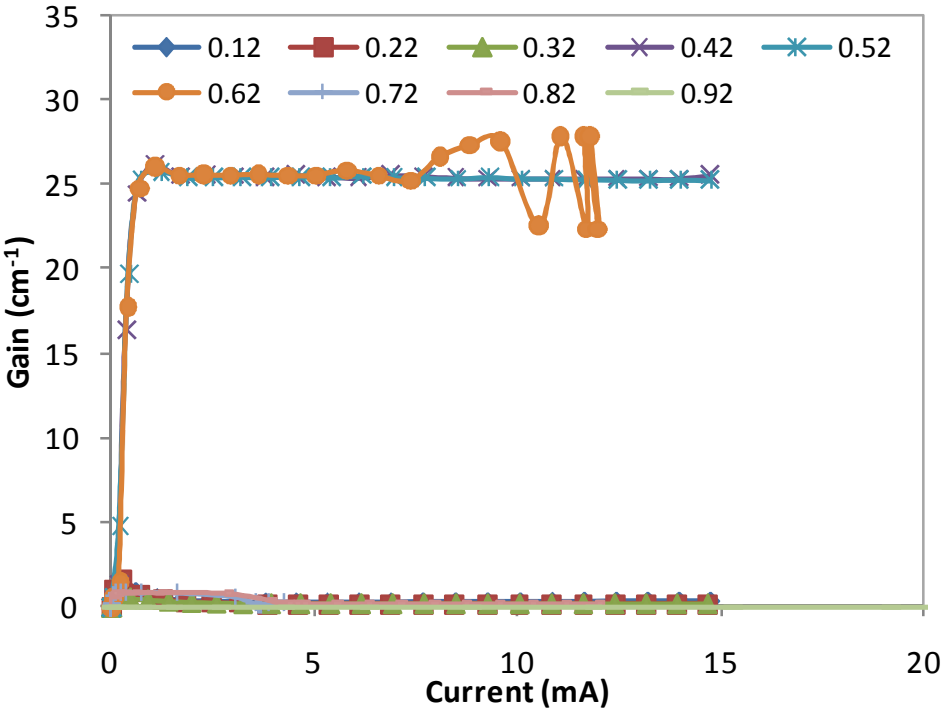

Figure 11. Gain-I curve for QW barrier x-comp variation.

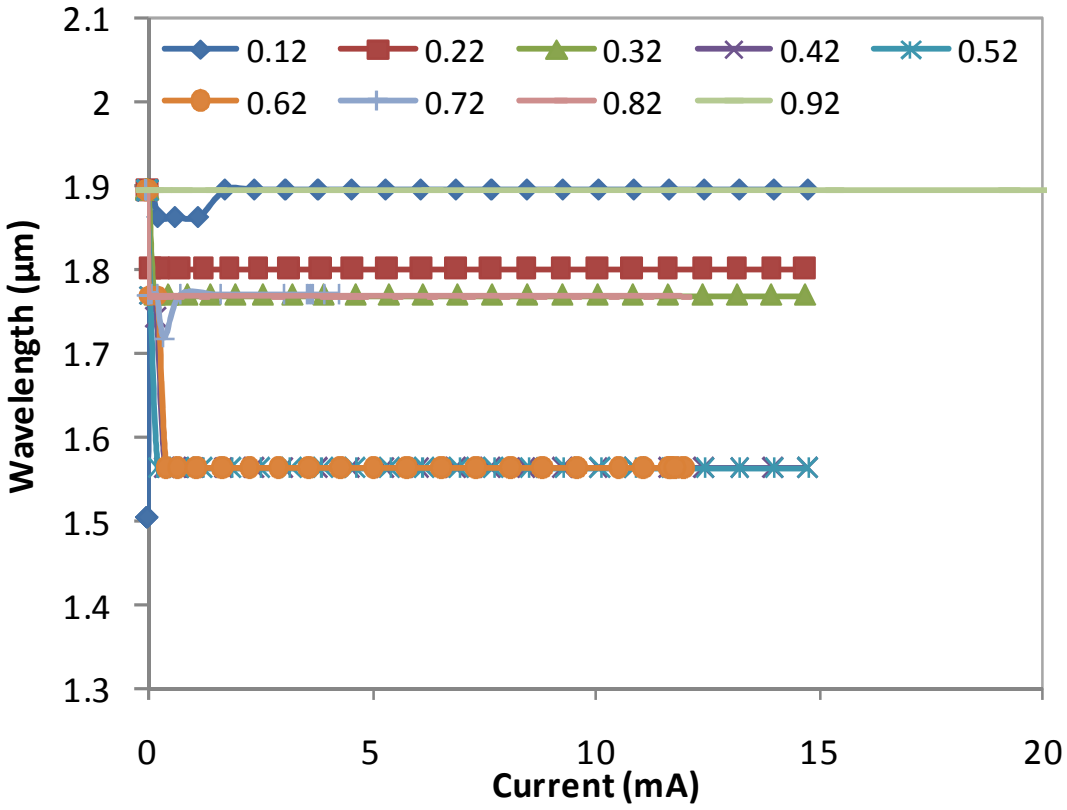

Figure 12. λ-I curve for QW barrier x-comp variation.

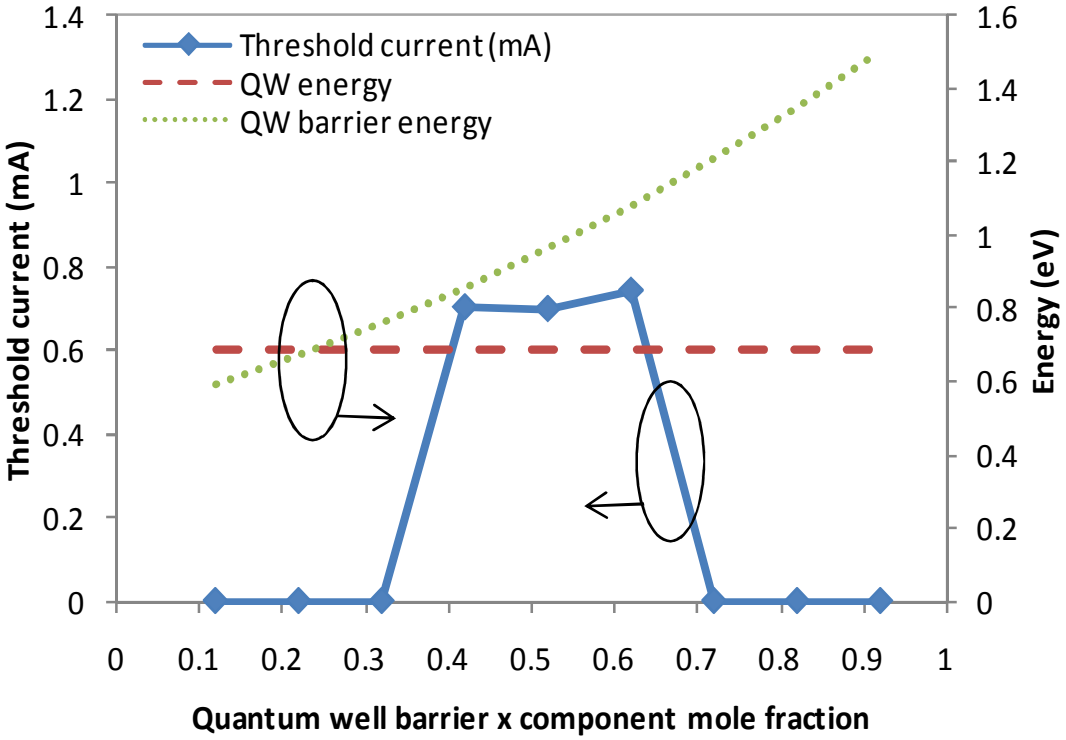

Figure 13. I_{th} (diamond bulleted line, left y-axis) and band gap energy (dotted and hyphenated lines, right y-axis) variation for different QW barrier x component mole fraction variation.

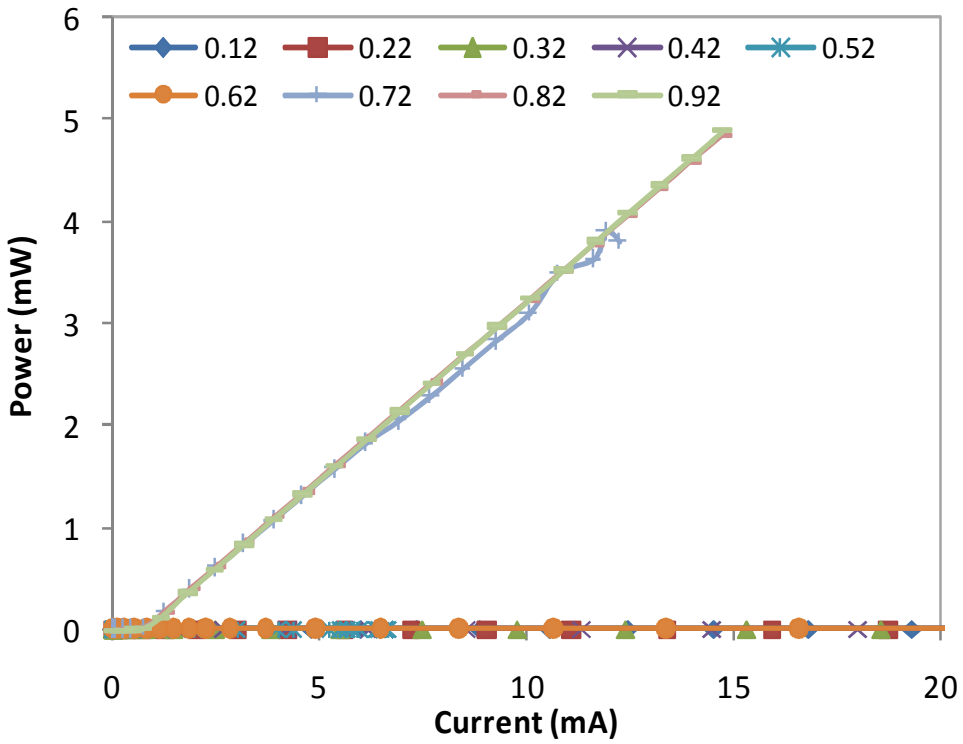

Figure 14. L-I curve for QW barrier y-comp variation.

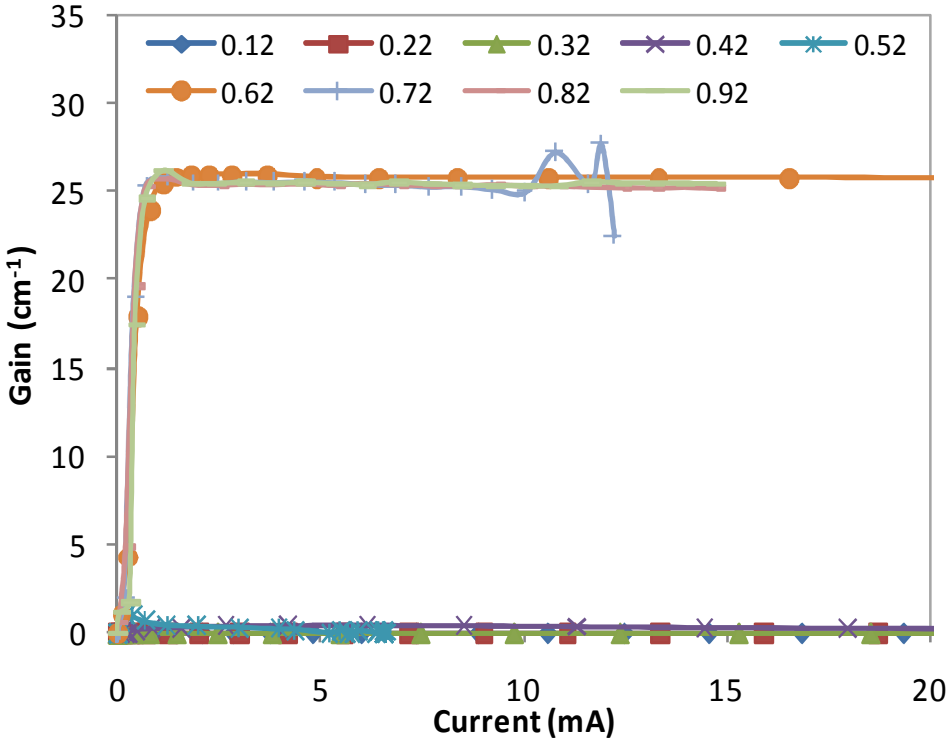

Figure 15. Gain-I curve for QW barrier y-comp variation.

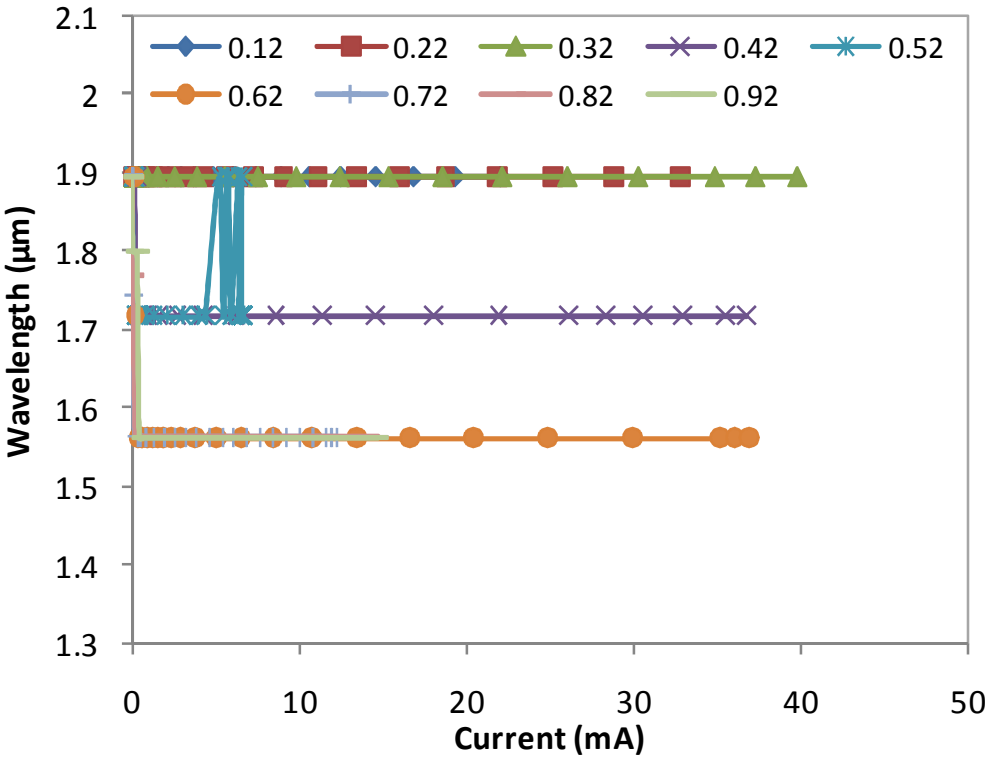

Figure 16. λ-I curve for QW barrier y-comp variation.

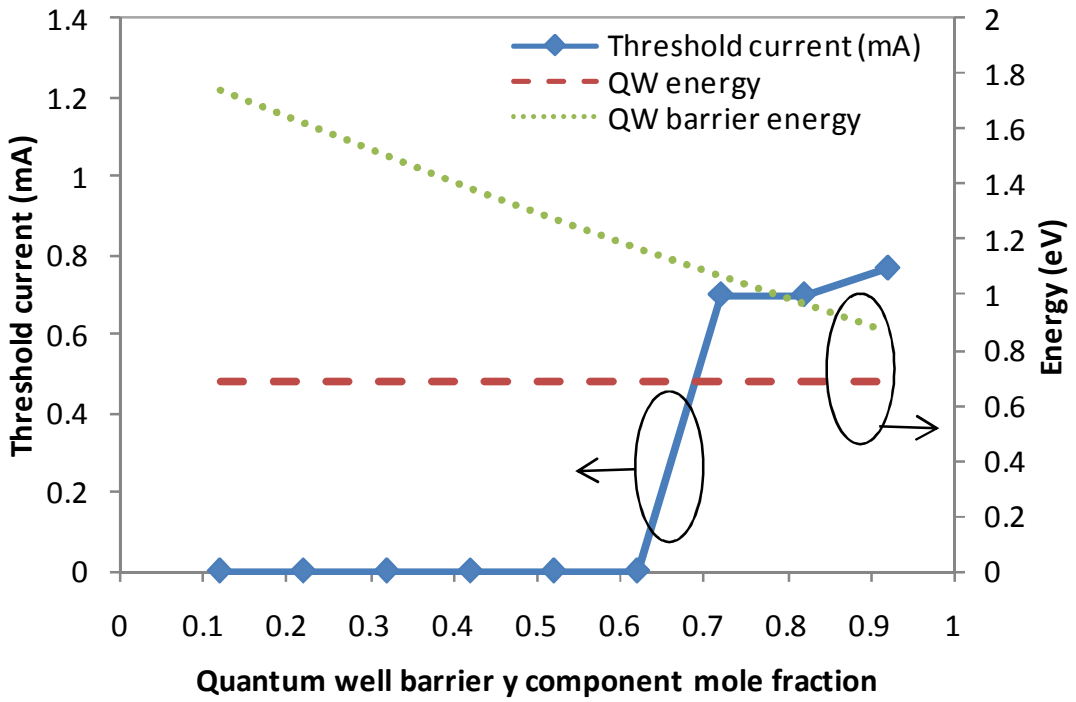

Figure 17. I_{th} (diamond bulleted line, left y-axis) and band gap energy (dotted and hyphenated lines, right y-axis) variation for different QW barrier y component mole fraction variation.

Table 1. Corresponding band-gap energy values for the multi-quantum well and multi-quantum well barrier for different combinations of the x and y component mole fractions as well as the threshold current.

x-mole fraction in QW, x_{QW}	y-mole fraction in QW, y_{QW}	x-mole fraction in QW barrier, x_{QWB}	y-mole fraction in QW barrier, y_{QWB}	QW band-gap energy, E_{QW} (eV)	QW barrier band-gap energy, E_{QWB} (eV)	Threshold current, I_{th} (mA)
0.14	0.82	0.52	0.82	0.61	0.96	0.27
0.24	0.82	0.52	0.82	0.68	0.96	0.70
0.34	0.82	0.52	0.82	0.77	0.96	0.49
0.24	0.92	0.52	0.82	0.59	0.96	0.70
0.24	0.82	0.42	0.82	0.68	0.85	0.70
0.24	0.82	0.62	0.82	0.68	1.08	0.74
0.24	0.82	0.52	0.72	0.68	1.06	0.70
0.24	0.82	0.52	0.92	0.68	0.86	0.77

multi-quantum well region. Table 1 summarizes the key values which enables lasing in the developed LW-VCSEL utilizing In(1-x)Ga(x)As(y)P(1-y) as the MQW material.

The lowest threshold current of 0.27 mA was achieved for the LW-VCSEL device with band-gap energy E_{QW} = 0.61 eV and E_{QWB} = 0.96 eV which corresponds to the mole fractions of x_{QW} = 0.14, y_{QW}=0.82, x_{QWB} = 0.52 and y_{QWB} = 0.82.

Conclusions

We have analyzed the effects of the multi quantum well and barrier material mole fraction towards the characteristics of a wafer-bonded InP-based LW-VCSEL by means of an industrial-based simulator. The results show that in order for lasing to occur the barrier material band-gap energy should be between 19 to 36% higher

than the quantum well material band-gap energy which utilizes InGaAsP as the active material. Beyond this range, no lasing occurs in the device. Increment of the quantum well band-gap energy shifts the resonance wavelength to higher values. The simulated device achieved lasing powers up to 4.9 mW with modal gain of 25 cm^{-1}, lasing wavelength of 1.56 µm and threshold current <0.8 mA for x_{QW}=0.24, y_{QW} = 0.82, x_{QWB} = 0.52 and y_{QWB} = 0.82.

ACKNOWLEDGEMENT

The authors would like to thank the Malaysian Ministry of Higher Education (MOHE) and University Kebangsaan Malaysia (UKM) for supporting the publication of this work under research grants UKM-GGPM-NBT-090-2010 and UKM-OUP-NBT-27-119/2011.

REFERENCES

Hofmann W (2011). Evolution of high-speed long-wavelength vertical-cavity surface-emitting lasers. Semicon. Sci. Technol., 26(2011): 1-11.

Hofmann W, Amann M-C (2008). Long-wavelength vertical-cavity surface-emitting lasers for high-speed applications and gas sensing. IET Optoelectronics, 2: 134-142.

Iizuka K (2002). Elements of Photonics, vol. II, Wiley-Interscience.

Kapon E, Sirbu A (2009). Power-efficient answer. Nature Photonics, 3: 27-29.

Karim A, Abraham P, Lofgreen D, Chiu Y-J, Piprek J, Bowers JE (2001). Wafer bonded 1.55 µm vertical-cavity lasers with continuous-wave operation up to 105 °C. Appl. Phys. Lett., 78: 2632-2634.

Karim A, Piprek J, Abraham P, Lofgreen D, Chiu Y-J, Bowers JE (2001). 1.55-µm vertical-cavity laser arrays for wavelength-division multiplexing. IEEE J. Sel. Top. Quantum Electron, 7: 178–183.

Kumarajah K, Ismail M, Menon PS, Shaari S, Majlis BY (2009a). Effect of MQW design parameters on the threshold current of an air-post 1.5 µm VCSEL. Pacific Rim Conference on Lasers and Electro-Optics, CLEO - Technical Digest , art. no. 5292073.

Kumarajah K, Ismail M, Menon PS, Shaari S, Majlis BY (2009b). Self-heating effects in a gain-guided vertical-cavity surface-emitting laser. 2009 Symposium on Photonics and Optoelectronics, SOPO 2009 , art. no. 5230301.

Li H, Iga K (2002). Vertical-Cavity Surface-Emitting Laser Devices. Springer.

Mehta M, Feezell D, Buell DA, Jackson AW, Coldren LA, Bowers JE (2006). Electrical design optimization of single-mode tunnel-junction-based long-wavelength VCSELs. IEEE J. Sel. Top. Quantum Electron., 42: 675-682.

Menon PS, Kandiah K, Ismail M, Majlis BY, Shaari S (2011). Comparison of mesa and device diameter variation in double wafer-fused multi quantum-well, long-wavelength, vertical cavity surface emitting lasers. Sains Malaysiana, 40(6): 631-636.

Menon PS, Kandiah K, Ismail M, Majlis BY, Shaari S (2010a). Long-wavelength MQW vertical-cavity surface emitting laser: effects of lattice temperature. J. Opt. Commun., 31(2): 81-84.

Menon PS, Kandiah K, Shaari S (2010b). Variation of MQW design parameters in a GaAs/InP-based LW-VCSEL and its effects on the spectral linewidth. J. Nonlin. Opt. Phys. Mater., 19(2): 209-217.

Menon PS, Kumarajah K, Bais B, Abdullah H, Majlis BY, Apte PR (2010c). Peak power and wavelength optimization of a double-fused LW-VCSEL. Proceedings of the 2010 IEEE International Conference on Semiconductor Electronics, ICSE2010 (Melaka), pp. 365-369.

Mereuta A, Surucceanu G, Caliman A, Iakovlev V, Sirbu A, Kapon E (2009). 10-Gb/s and 10-km error-free transmission up to 100 °C with 1.3 µm wavelength wafer-fused VCSELs. Optics Express 17: 12981-12986.

Qi C, Shi X, Wang G (2010). Thermal circuit model of MQW VCSEL Laser. Proceedings of the 2010 International Conference on Microwave and Millimeter Wave Technology (ICMMT), pp. 1498-1501.

Silvaco International (2010), ATLAS User's Manual, Version 5.16.3.R. SILVACO International Incorporated.